Regimes of Biomolecular-Ultrasmall Nanoparticle Interactions

Luca Boselli*‡[a], Ester Polo‡[a], Valentina Castagnola[a] , Kenneth A. Dawson*[a]

Abstract: Ultrasmall nanoparticles (USNPs), usually defined as NPs with core in the size range 1-3 nm, are a class of nanomaterials which show unique physicochemical properties, often different from larger NPs of the same material. Moreover, there are also indications that USNPs might have distinct properties in their biological interactions. For example, recent *in vivo* experiments suggest that some USNPs escape the liver, spleen and kidney, in contrast to larger NPs that are strongly accumulated in the liver. In this work we present a simple approach to study the biomolecular interactions at the USNPs bio-nano interface, opening up the possibility to systematically link these observations to microscopic molecular principles.

In the last two decades, nanoparticles (NPs) have been intensively investigated for their potential in a wide range of applications, including biomedicine.[1] Ultrasmall NPs (USNPs, considered core size 1-3 nm) can behave significantly different from “larger” NPs of the same material, sometimes presenting unique magnetic, electrical, optical and catalytic properties.[2] In the last 10 years, the biological interactions of NPs have been extensively studied, showing that, when exposed to biological media, all NPs (even with specially prepared surfaces) interact with biomolecules (proteins, lipids, etc.) that adsorb onto their surface, forming the so-called “biomolecular corona”.[3] This new biological identity can determine the final fate of NPs in living organisms.[4]

Most early *in vivo* biodistribution studies report a common tendency of NPs to accumulate extensively in the liver, with the attendant potential for toxicity.[5] This tendency remains surprisingly high (30-60 %) even with specialized surface coatings and may have significant implications for long term toxicity and actively targeted drug delivery using NPs.[6] However, several reports also suggest that USNPs accumulate less in the liver.[7] It has been reported that 2 nm glutathione-coated gold nanoparticles (GNPs) exhibit efficient renal clearance, with approximately 4 % of the NPs accumulated in the liver, 9 % in the kidney, 5 % in the lung and 0.3 % in the spleen.[8] Moreover, it has been reported that luminescent 2.7 nm (core size) tiopronin-capped GNPs accumulate in the liver and kidneys.[7b] On the other hand, several examples of NPs of sizes less than 2 nm are known to exhibit much less liver accumulation.[7c]

We certainly expect size effects themselves to be significant in, for example, renal clearance where glomerular filtration is known to be size dependent and indeed appears to have a filtration-size threshold. As the particle size becomes very small, the interactions with biomolecules are generally expected to diminish, and those that remain may lead to quite different organizations in which multiple particles interact with a single protein, rather than the reverse.[9] The fact that the overall biodistribution could result from different size-dependent effects (physical filtration and biomolecular associations), combined with the absence of any generally accessible and systematic way of studying the nature (or even presence) of these biomolecular associations, makes it difficult to progress systematic understanding of these effects. Several interesting studies have clarified aspects of the biomolecular interactions with ultrasmall nanoparticles.[10]

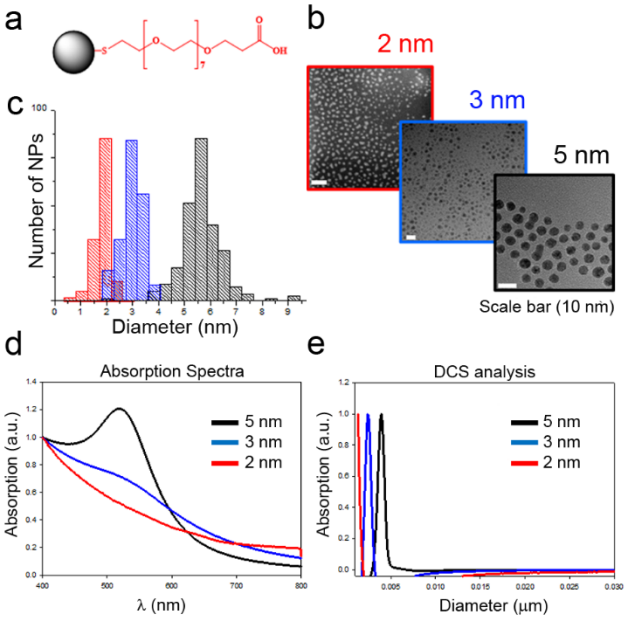

Figure 1. Characterization of 2, 3 and 5 nm GNP-PEG-COOH: a) Schematic ligand representation; b) TEM micrographs and c) TEM size distribution; d) Absorption spectra; e) Size distribution as measured by DCS analysis.

Here, in order to make contact with the *in vivo* studies we focus on consequences of particle size and surface on the interactions between USNPs and concentrated biological fluids. We investigate the transition regime between examples in which several proteins can bind relatively irreversibly to the particle, and those where all of the proteins are in rapid exchange, and none bind strongly. We find this transition to be quite sensitively

[a] Centre for BioNano Interaction
University College Dublin, School of Chemistry
Belfield, Dublin 4
[*] Prof. K. A. Dawson, Dr. L. Boselli
E-mail: kenneth.a.dawson@cbni.ucd.ie, luca.boselli@cbni.ucd.ie
[‡] These authors contributed equally.

Supporting information for this article is given via a link at the end of the document.

dependent on small changes in size and surface chemistry. We chose gold as an illustrative system and note the convenience it provides in practical biodistribution studies.[11] Three representative sizes have been chosen as models: 2 nm GNP (ultrasmall size range), 3 nm GNP and 5 nm GNP, the latter typically considered beyond the ultrasmall range. Moreover, an additional series of 2 nm GNPs with different surface functionalities has been included in the study in order to investigate the role of surface charge/chemistry (see Table 1).

A family of negatively charged monodisperse GNPs functionalized with SH-PEG(7)-COOH ligands (GNP-PEG-COOH) was synthesized and characterized (Figure 1, Figures S1, S2, S8a and S10).

	Name	Ligand structure	Size
GNP	PEG-COOH	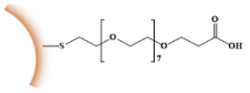	2 nm 3 nm 5 nm
	αGalPEGSuc	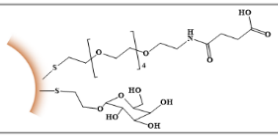	2 nm
	Tiopronin	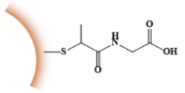	2 nm
	Glutathione	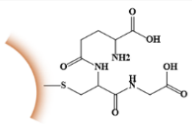	2 nm
	αGalPEGAmino	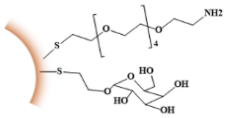	2 nm

Table 1. Summary of the GNPs used in this study including size and schematic representation of the ligand chemical structure

Clearly, the approaches previously developed to study biomolecular corona formation on larger NPs (10 - 100 nm) are no longer appropriate for the study of USNPs which can be of comparable size, or even smaller than the biomolecules themselves. Thus the ultrasmall range is located at the edge (or below) of resolution limits of the routinely employed instruments for NPs characterization such as dynamic light scattering (DLS), differential centrifugal sedimentation (DCS) or transmission electron microscopy (TEM) and to isolate the NP-protein complexes is extremely challenging. Analytical ultracentrifugation (AUC) and Fluorescence correlation spectroscopy (FCS) are very useful and sophisticated techniques have been successfully employed to investigate USNP-protein interactions, mainly using single proteins.[12]

We used a series of gel assays for in situ investigation of biomolecules-USNPs interactions.[13] The GNP-PEG-COOH samples (5 nm, 3 nm and 2 nm) were normalized by surface area and exposed to human plasma (HP). Samples were then incubated with 70 % v/v of HP to ensure protein content was in excess. The mixtures were then incubated for 30 minutes and loaded into the wells of an agarose gel next to the corresponding control (NP suspension in PBS).

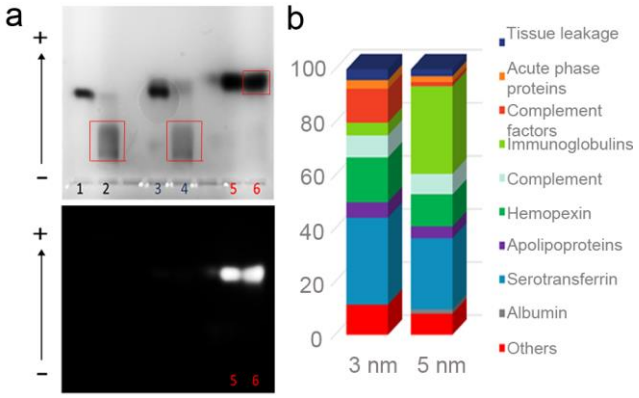

Figure 2. a) 1 % agarose gel-assay in a native buffer. The numbered lanes refer to 5 nm GNP-PEG-COOH in PBS (1) and in HP (2), 3 nm GNP-PEG-COOH in PBS (3) and in HP (4), 2 nm GNP-PEG-COOH in PBS (5) and in HP (6). Below, the image captured by fluorescence detection mode. Note: only 2 nm GNP-PEG-COOH exhibit fluorescence. b) Mass spectrometry analysis of 3 nm and 5 nm GNP-PEG-COOH corona complexes isolated by agarose gel electrophoresis.

We observed (Figure 2) that for 5 nm (lanes 1 and 2) and 3 nm (lanes 3 and 4) GNP-PEG-COOH NP-protein interactions led to significant changes in NPs mobility (as can be seen from the smear in lane 2 and 4). In contrast, 2 nm GNP-PEG-COOH particles exhibit few signs of protein interaction. Different voltage and gel pore size conditions are reported in Figures S3-5 showing similar effects, leading us to conclude that larger particles form more conventional protein corona complexes (illustrated by the evident shift in mobility of the bio-nano complex compared to free NPs), while smaller ones do not. In order to gain further insight into this process, we recorded a full video of NP progression through the agarose gel. For this experiment, a 3.5 % agarose gel was used in order to increase the resolution and observe smaller differences (see Figure S5). For instance, 2 nm GNP-PEG-COOH demonstrated slightly lower electrophoretic mobility in comparison to the NP control in PBS, at very early time points. This difference can be mainly observed when the NPs enter in the gel (Figure S5). In addition, for the gels in Figures S6-7, gold particle-protein complexes were isolated by excising the band of interest in the gel and subjected to mass spectrometry (MS) analysis to identify the proteins involved (see Figure 2b and Table S1). It is noteworthy that there is considerable smearing of electrophoresed gold-biomolecular complexes, possibly reflecting that, for small NP sizes, the interaction of so many different proteins (roughly 3700) generates significant heterogeneity in

complex size and composition. It is, however, striking that the qualitative nature of the interactions should change so precipitously around a specific size (2 nm), with highly heterogeneous complexes forming in the vicinity of this transition.

Figure 3. CCD experiment in 1 % agarose gel including samples: 2 nm GNP-PEG-COOH in PBS (1) and in HP (2), HP stained with SYPRO® orange dye (3).

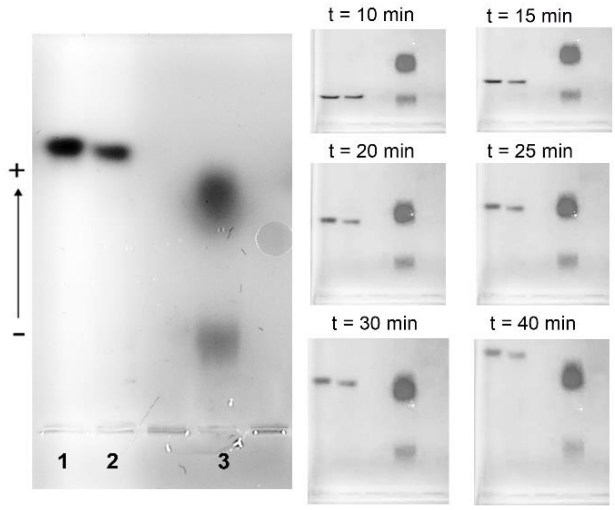

The observation that corona lifetimes should decrease with size is both intuitively obvious, and also consistent with earlier theoretical observations.[14] However, it is intriguing that transient particle-protein associations with lifetimes shorter than gel band resolution times still lead to modified mobility whose consequences can be observed in “cyclic capture and dissociation” (CCD) dynamics.[15] As shown in Figure 3 (lane 1 NPs alone, lane 3 HP alone and lane 2 HP first run into the gel, and then ‘chased’ by nanoparticles) while the long term (45 mins) outcome suggests a modest effect on overall (averaged) particle mobility, the temporal evolution of the CCD dynamics is much more revealing. Thus, (see Figure 3) at early stages (before 10 mins) the higher electrophoretic mobility of the chasing NPs allows them to overtake the first of the two major HP bands, which they appear to pass without significant retardation. However NPs reach the lower molecular weight plasma region, where they are strongly retarded (Figure 3, t = 20 - 25 min), and follow the protein band until, after around 35 mins, they move independently again. We have found that these effects are typical of particles (and particle surfaces) that are believed to have transient associations, and the retardations were (in molecular systems)[15] interpreted as a consequence of repetitive binding and unbinding of particle and protein within the band, though in our more complex system deduction of explicit affinities will be more challenging.

We stress that the transition between the conventional long-lived ‘hard corona’ complexes and these non-interacting (or ‘pseudo-corona’) scenarios is a consequence of the weakening particle-biomolecular interactions, which is parameterized by both particle size and particle surface. This surface chemistry effect may be illustrated using identical core particles but different ligands (Table 1, characterisation reported in Figures S8-10 and Table S2). Thus (Figure 4) tiopronin (2 nm GNP-tiopronin, lane 5, 6) and glutathione ligands (2 nm GNP-glutathione lanes 7, 8) show significant biomolecular corona interactions, whereas PEG-type ligands (2 nm GNP-PEG-COOH, lanes 1, 2 and 2 nm GNP-α GalPEGSuc, lanes 3, 4) do not. That outcome is consistent with expectations and may reflect the fact that the former have shorter chain lengths and higher net charge.[16]

Furthermore, as expected, positively charged 2 nm GNP-αGalPEGAmino (similar to GNP-αGalPEGSuc but with opposite charge) also interact strongly with plasma proteins (lanes 9, 10).

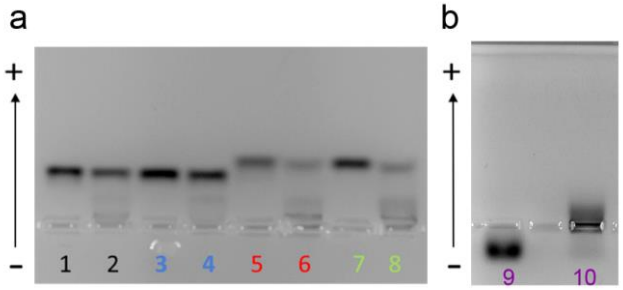

Figure 4. 3.5 % agarose gel-shift assay experiment including samples: a) 2 nm GNP-PEG-COOH in PBS (1) and in HP (2), 2 nm GNP- αGalPEGSuc in PBS (3) and in HP (4), 2 nm GNP-tiopronin in PBS (5) and in HP (6), 2 nm GNP-glutathione in PBS (7) and in HP (8); b) 2 nm GNP-αGalPEGAmino in PBS (9) and in HP (10).

It is noteworthy that in addition to the smearing observed in Figure 4, there is evidence of a bimodal behaviour (see Figure S11) in which some proteins bind and others do not (Figure 4 lanes 6, 8). This may arise as a consequence of particle heterogeneity (for example ligand density or size), then strongly highlighted by differential protein binding. These observations are consistent with our experience, as well as being of some significance in planning the fabrication of ultrasmall nano-drugs.

When methods applied in new ways one should exercise caution.[17] For instance, while we have sought to study different conditions (electrical field, pore size, etc.) to assure ourselves that this does not in itself greatly influence the exchange process (see Figure S3). With these reservations we may summarise as follows. Firstly, size (in combination with surface) may be used to control, indeed even nearly eliminate, long-lived interactions between particle and the biomolecular environment. This suggests a transition between the regime where the particle corona identity is relatively fixed [3b] to one where it fluctuates rapidly. Certainly, this will lead to quite distinct biological outcomes, potentially interpolating between (non-associating) molecular drug, and more conventional nanoparticle activity, all of which may be ‘pre-screened’ prior to biological or *in vivo* studies.

We also stress that, from a practical perspective, in this ultra-small size range, even very small particle variations can lead to quite different biophysical interactions, reinforcing the role of 'particle quality' for this regime.

Finally, we also note the interesting possibility, enabled by the capacity to purposefully engineer the particle corona, to form transient complex interactions, could lead to a much richer range of 'particle-biomolecule' receptor target interactions, qualitatively different from molecules or larger particles. The degree to which receptor recognition paradigms could thereby be enriched is an interesting topic for further considerations.

Acknowledgements

We gratefully acknowledge the UCD Conway Mass Spectrometry Facility and the Trinity College CRANN Advanced Microscopy Laboratory facility. Acknowledges to Jennifer Cookman for the help in the TEM analysis. We acknowledge Midatech Pharma for the helpful support and scientific discussions L.B. acknowledges the financial support of the EU H2020 Nanofacturing project (grant agreement n°646364). E.P. and K.A.D. acknowledge Science Foundation Ireland (SFI) Principal Investigator Award 298 (agreement n°12/IA/1422). V.C. acknowledges the Irish Research Council (GOIPD/2016/128).

Keywords: ultrasmall • protein - corona • gold • nanoparticles • gel-assay.

[1] a) E. C. Dreaden, A. M. Alkilany, X. Huang, C. J. Murphy, M. A. El-Sayed, *Chem. Soc. Rev.* **2012**, 41, 2740-2779; b) M. Ferrari, *Nat. Rev. Cancer* **2005**, 5, 161-171; c) J. Shi, P. W. Kantoff, R. Wooster, O. C. Farokhzad, *Nat. Rev. Cancer* **2016**, advance online publication.

[2] a) B. H. Kim, M. J. Hackett, J. Park, T. Hyeon, *Chem. Mater.* **2013**, 26, 59-71; b) K. Zarschler, L. Rocks, N. Licciardello, L. Boselli, E. Polo, K. P. Garcia, L. De Cola, H. Stephan, K. A. Dawson, *Nanomed. Nanotech. Biol. Med.* **2016**, 12, 1663-1701.

[3] a) T. Cedervall, I. Lynch, M. Foy, T. Berggård, S. C. Donnelly, G. Cagney, S. Linse, K. A. Dawson, *Angew. Chem., Int. Ed*. **2007**, 46, 5754-5756; b) T. Cedervall, I. Lynch, S. Lindman, T. Berggård, E. Thulin, H. Nilsson, K. A. Dawson, S. Linse, *Proc. Natl. Acad. Sci. U. S. A*. **2007**, 104, 2050-2055; c) M. P. Monopoli, C. Aberg, A. Salvati, K. A. Dawson, *Nat. Nanotechnol.* **2012**, 7, 779-786.

[4] a) A. Salvati, A. S. Pitek, M. P. Monopoli, K. Prapainop, F. B. Bombelli, D. R. Hristov, P. M. Kelly, C. Åberg, E. Mahon, K. A. Dawson, *Nat. Nanotechnol.* **2013**, 8, 137-143; b) C. D. Walkey, J. B. Olsen, F. Song, R. Liu, H. Guo, D. W. H. Olsen, Y. Cohen, A. Emili, W. C. W. Chan, *ACS Nano* **2014**, 8, 2439-2455.

[5] a) E. Sadauskas, G. Danscher, M. Stoltenberg, U. Vogel, A. Larsen, H. Wallin, *Nanomed. Nanotech. Biol. Med*. **2009**, 5, 162-169; b) G. Sonavane, K. Tomoda, K. Makino *Colloids Surf., B* **2008**, 66, 274-280.

[6] S. Wilhelm, A. J. Tavares, Q. Dai, S. Ohta, J. Audet, H. F. Dvorak, W. C. W. Chan, *Nat. Mater. Rev*. **2016**, 1, 16014.

[7] a) J. Liu, M. Yu, C. Zhou, S. Yang, X. Ning, J. Zheng, *J. Am. Chem. Soc*. **2013**, 135, 4978-4981; b) W. Poon, A. Heinmiller, X. Zhang, J. L. Nadeau, *J. Biomed. Opt*. **2015**, 20, 066007-066007; c) X.-D. Zhang, Z. Luo, J. Chen, S. Song, X. Yuan, X. Shen, H. Wang, Y. Sun, K. Gao, L. Zhang, *Sci. Rep*. **2015**, 5; d) X.-D. Zhang, D. Wu, X. Shen, P.-X. Liu, F.-Y. Fan, S.-J. Fan, *Biomaterials* **2012**, 33, 4628-4638.

[8] C. Zhou, M. Long, Y. Qin, X. Sun, J. Zheng, *Angew. Chem., Int. Ed*. **2011**, 123, 3226-3230.

[9] Z. J. Deng, M. Liang, I. Toth, M. J. Monteiro, R. F. Minchin, *ACS Nano* **2012**, 6, 8962-8969.

[10] D.F. Monayo, K. Saha, G. Prakash, B. Yan, H. Kong, M. Yazdani, V.M. Rotello. ACS Nano 2014, 8, 6748-6755

[11] a) R. Gromnicova, H. A. Davies, P. Sreekanthreddy, I. A. Romero, T. Lund, I. M. Roitt, J. B. Phillips, D. K. Male, *PLOS ONE* **2013**, 8, e81043; b)N. Khlebtsov, L. Dykman, *Chem. Soc. Rev*. **2011**, 40, 1647-1671; c) J. Lipka, M. Semmler-Behnke, R. A. Sperling, A. Wenk, S. Takenaka, C. Schleh, T. Kissel, W. J. Parak, W. G. Kreyling, *Biomaterials* **2010**, 31, 6574-6581.

[12] a) A. Bekdemir, F. Stellacci, *Nat. Comm*. **2016,** 7, 13121; b) R. P. Carney, J. Y. Kim, H. Qian, R. Jin, H. Mehenni, F. Stellacci, O. M. Bakr, *Nat. Commun.* **2011**, 2, 335; c) C. Rocker, M. Potzl, F. Zhang, W. J. Parak, G. U. Nienhaus, *Nat. Nanotechnol.* **2009,** 4, 577-580.

[13] a) C.A. Lin, R.A. Sperling, J.K., Li, T.Y. Yang, P.Y. Li, M. Zanella, W.H., Chang, W.J. Parak. Small 2008, 4, 334-41. b) C.A. Lin, T.Y. Yang, C.H. Lee, S. H. Huang, R.A., Sperling, M. Zanella, J. K. Li, J.L. Shen, H.H. Wang, H. Yeh, W.J. Parak, W.H. Chang. ACS Nano, 2009, 3, 395-401

[14] a) S. H. D. P. Lacerda, J. J. Park, C. Meuse, D. Pristinski, M. L. Becker, A. Karim, J. F. Douglas, *ACS Nano* **2010**, 4, 365-379; b) H. Lopez, V. Lobaskin, *J. Chem. Phys*. **2015**, 143, 243138.

[15] B. P. Belotserkovskii, B. H. Johnston, *Biophys. J*. **1997**, 73, 1288-1298.

[16] a) S. Ashraf, et al., *Nanoscale* **2016**; b) K. Pombo-García, et al., *Chem. Nano. Mat***. 2016**, 2, 959-971; c) S. Schöttler, G. Becker, S. Winzen, T. Steinbach, K. Mohr, K. Landfester, V. Mailänder, F. R. Wurm, *Nat. Nanotechnol*. **2016,** 11, 372-377.

[17] C. Holm. Traffic and Granular Flow´03, 2005, 475-488.

Entry for the Table of Contents (Please choose one layout)

Layout 2:

COMMUNICATION

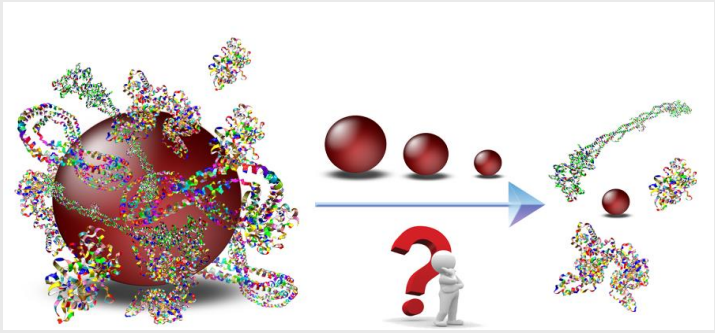

Luca Boselli, Ester Polo, Valentina Castagnola, Kenneth A. Dawson[a]*

Regimes of Biomolecular-Ultrasmall Nanoparticle Interactions.

Biomolecular interactions at the ultrasmall nanoparticle bio-interface

Supporting Information

Contents

1 Materials 7

2 Experimental Section 7

2.1 Synthesis of Nanoparticles 7

2.1.1 Preparation of the ultrasmall gold nanoparticles 7

2.1.2 Synthesis of 3 nm GNP-PEG-COOH 8

2.1.3 Synthesis of 5 nm GNP-PEG-COOH 8

2.2 Material Characterization 9

2.2.1 UV-visible spectroscopy 9

2.2.2 Differential Centrifugal Sedimentation 9

2.2.3 Dynamic Light Scattering 9

2.2.4 Transmission electron Microscopy 9

2.2.5 Nuclear Magnetic Resonance 9

2.3 Gel Electrophoresis 9

2.3.1 Agarose electrophoresis. 10

2.3.2 Polyacrylamide gel electrophoresis (PAGE) 10

2.3.3 Mass spectrometry 10

3 Supplementary Figures 12

4 References 24

1 Materials

All chemicals were of highest grade available and used as received. Gold(III) chloride trihydrate (520918), N-(2-Mercaptopropionyl)glycine (280968), O-(2-Carboxyethyl)-O′-(2-mercaptoethyl) heptaethylene glycol (SH-PEG-COOH, 672688), PBS Tablets (P4411), Trizma® base (T1503), Glycine (G8898), Ammonium persulfate (A3678), Ethylenediaminetetraacetic acid disodium salt dehydrate EDTA (252352), Sodium dodecyl sulfate SDS (L3771), N,N,N′,N′-Tetramethylethylenediamine TEMED (T9281), Sucrose (m117), Dodecane (D22110), Acrylamide/bis-acrylamide 40% solution (A7802), DTT-Dithiothreitol (D5545), Ethanol (32294-2), Methanol (24229-2), Trisodium citrate dihydrate (S1804), Tannic acid (16201) and potassium carbonate (P4379) were purchased from Sigma-Aldrich.

In addition: PVC calibration standard 483 nm (PVC000476) were purchased from Analytik Ltd., Color Plus Pre-stained Protein Ladder, Broad Range (10-230 kDa) (P7711S) and Blue Loading Buffer for SDS-PAGE were ordered from New England Bio-Labs (cat. no. B7703S), Micro BCA Protein Assay Kit and Pierce ECL (cat. no. 23235) was purchased from Thermo Scientific., 2D Silver Stain Kit II [Daiichi] (167997) was purchased from Insight biotechnology, SYPRO® orange was purchased from ThermoFisher Scientific, MetaPhor® Agarose (50180) was purchased by LONZA.
Human Plasma was obtained from the Irish Blood Transfusion Service. Total protein content was estimated to be ca. 80 mg/ml by micro bicinchoninic acid assay (µ-BCA). Plasma was defrosted and centrifuged at 16200 RCF for 3 min at prior to use.

2 nm GNP-Glutathione, GNP-aGalPEGSuc and GNP-aGalPEGAmino have been supplied by MidatechPharma®.

2 Experimental Section

2.1 Synthesis of Nanoparticles

2.1.1 Preparation of the ultrasmall gold nanoparticles

2.1.1.1 Synthesis of 2 nm GNP-PEG-COOH

2 nm GNP-PEG-COOH have been synthesized by using a modification of the method reported in literature by Templeton and co-workers.[1] In a 50 mL round bottom flask $HAuCl_4$ (0.078 g, 0.20 mmol) and O-(2-Carboxyethyl)-O′-(2-mercaptoethyl) heptaethylene glycol (SH-PEG-COOH (0.55 g, 1.2 mmol) were dissolved in 9 mL of 6:1 methanol/acetic acid. The solution was stirred for 5 minutes at RT. While the solution was vigorously stirring $NaBH_4$ (0.15 g, 4 mmol) in 3.8 mL of MilliQ water was added drop by drop. The solution become immediately of dark-brown color characteristic of the ultrasmall gold nanoparticles. The reaction was finally stirred for further 30 minutes. The MeOH was removed by rotary evaporation. 5-10 mL of MilliQ water were added to the concentrate water solution containing the nanoparticles. This diluted solution was filtered through a 0.2 µm Millipore® syringe filter and then purified by using dialysis technique (membrane MWCO = 3000) in order to eliminate

the unreacted ligands and the inorganic salts formed during the reaction. The solution was finally concentrated using a centrifugation filter (10,000 MWCO) to a volume of 5-10 mL in order to have a concentration of 8-10 mg/mL.

2.1.1.2 Synthesis of 2 nm GNP-Tiopronin

2 nm GNP-Tiopronin has been synthesized as reported by Templeton and co-workers. [1] In a 50 mL round bottom flask $HAuCl_4$ (0.078 g, 0.20 mmol) and N-(2-mercaptopropionyl)glycine (0.19 g, 1.2 mmol) were dissolved in 9 mL of 6:1 methanol/acetic acid. The solution was stirred for 5 minutes at RT. While the solution was vigorously stirring $NaBH_4$ (0.15 g, 4 mmol) in 3.8 mL of MilliQ water was added drop by drop. The solution become immediately of dark-brown color characteristic of the ultrasmall gold nanoparticles. The reaction was finally stirred for further 30 minutes. The MeOH was removed by rotary evaporation. 5-10 mL of MilliQ water were added to the concentrate water solution containing the nanoparticles. This diluted solution was filtered through a 0.2 µm Millipore® syringe filter and then purified by using dialysis technique (membrane MWCO = 3000) in order to eliminate the unreacted ligands and the inorganic salts formed during the reaction. The solution was finally concentrated using a centrifugation filter (10,000 MWCO) to a volume of 5-10 mL in order to have a concentration of 8-10 mg/mL.

2.1.2 Synthesis of 3 nm GNP-PEG-COOH

3 nm GNP-PEG-COOH have been synthesized by using a modification of the method reported in literature.[2] In a 100 mL round bottom flask, 10 mL of aqueous reducing solution containing trisodium citrate (25 mg, 0.085 mmol), tannic acid (25 mg, 0.015 mmol) and potassium carbonate (5 mg, 0.036 mmol) was prepared and pre-heated to 60 °C. Separately, $HAuCl_4$ (5 mg, 0.013 mmol) was dissolved in 40 mL of water and heated to 60 °C. The gold precursor solution was rapidly added to the reducing solution under vigorous stirring, then the mixture was heated under reflux to the boiling point for 2 min and finally cooled to RT by using an ice-bath. Afterwards, the pH of the colloidal dispersion was adjusted to 8.5 by using aqueous NaOH (500 mM). An orange-brown dispersion was obtained. O-(2-Carboxyethyl)-O′-(2-mercaptoethyl) heptaethylene glycol ligand (2.5 mg**,** 0.0055 mmol) was dissolved in 1 mL of MilliQ water and added to the NP suspension at RT under stirring.[3] After 12 hours, the carboxylated gold nanoparticles were washed 3 times and concentrated with centrifugal filter units (10,000 MWCO).The solution was filtered through a 0.2 µm Millipore® syringe filter and then purified as reported for 2 nm GNP-PEG-COOH.

2.1.3 Synthesis of 5 nm GNP-PEG-COOH

5 nm GNP-PEG-COOH have been synthesized by using a modification of the method reported in literature.[2] In a 100 mL round bottom flask, $HAuCl_4$ (5 mg, 0.013 mmol) was dissolved in 40 mL of water and heated to 60 °C. Separately, 10 mL of aqueous reducing solution containing trisodium citrate (20 mg, 0.068 mmol), tannic acid (5mg, 0.003 mmol) and potassium carbonate (1.75 mg, 0.013 mmol) was prepared and also pre-heated to 60 °C. Subsequently, the reducing solution was rapidly added to the gold precursor solution under vigorous stirring, then the mixture was heated under reflux to the boiling point for 2 min and finally cooled to RT by using an ice-bath. Afterwards, the pH of the colloidal dispersion was adjusted to 8.5 by using aqueous NaOH (500 mM). An orange-red dispersion is obtained. O-

(2-Carboxyethyl)-O′-(2-mercaptoethyl)heptaethylene glycol ligand (2.5 mg, 0.0055 mmol) was dissolved in 1 mL of MilliQ water and added to the NP suspension at RT under stirring.[3] After 12 hours, the carboxylated gold nanoparticles were washed 3 times and concentrated with centrifugal filter units (10,000 MWCO).The solution was filtered through a 0.2 µm Millipore® syringe filter and then purified as reported for 2 nm GNP-PEG-COOH.

Gold particles were characterized by DCS, UV-Vis spectroscopy, DLS and TEM.

2.2 Material Characterization

2.2.1 UV-visible spectroscopy

UV-visible spectroscopy was performed on a Cary 600i UV-visible spectrophotometer using a 1 cm path length Hellma quartz cells, measuring in the 200-800 nm range.The absence of the surface Plasmon resonance band suggest that the dimension of the gold core of the nanoparticles is $\leq$ 2 nm. The concentration of the NPs has been established by using the absorption spectra as described in literature by Haiss et al.[4]

2.2.2 Differential Centrifugal Sedimentation

Differential Centrifugal Sedimentation (DCS) analysis of gold nanoparticles was performed using a CPS Disk Centrifuge DC2400. The measurements were carried out using an 8-24% sucrose density gradient in MilliQ water, with a disc speed set to 24000 rpm while monitoring the 1-500 nm range. Each particle size measurement was calibrated using a PVC standard of nominal diameter 483 nm. 100 µL of standard was injected before each measurement to calibrate the instrument. 100 µL of particles were injected and analysed by DCS.

2.2.3 Dynamic Light Scattering

ζ potential of the NPs suspension was measured by Zetasizer Nano ZS by using a disposable capillary zeta cell. ζ potential measurements reported are an average of three independent measurements, with each measurement consisting of an accumulation of 11 runs.

2.2.4 Transmission electron Microscopy

Samples for HR-TEM and STEM imaging were prepared by evaporating ca. 10 µL of the nanoparticle suspension onto a NetMeshTM Lacey Carbon 300 mesh copper grid or holy carbon grid. FEI Titan TEM and FEI Tecnai G2 20 Twin TEM operating at accelerating voltage of 200 kV were utilized for imaging.

2.2.5 Nuclear Magnetic Resonance

The samples were freeze dried overnight and re-suspended in D_2O. ^{1}H-NMR spectra were recorded at 298 K on Varian Inova 300MHz Spectrometer or Varian NMR System 400MHz Spectrometer.

2.3 Gel Electrophoresis

Gel-electrophoresis was applied to investigate size distribution of the GNPs. Gel-shift assays were performed by using MetaPhor® Agarose and Native gels prepared at different %

following the procedure indicated by the supplier. In addition, denaturalized gel electrophoresis was applied to investigate the protein profile.

2.3.1 Agarose electrophoresis.

Different percentages of agarose gel were prepared by using MetaPhor® Agarose from Lonza in 1 x native buffer (25mM Tris-HCl and 25mM Glycine, pH 8.3). The 1x native running buffer solution was filtrated and degassed before to be used to make the gels. The samples were diluted by using a native running buffer containing 70% of glycerol, loaded in the gel and run using different voltage as difference of potential, using a Mini-Sub Cell GT Cell electrophoresis system from Bio-Rad.

2.3.2 Polyacrylamide gel electrophoresis (PAGE)

In order to investigate the protein adsorption of 3 nm GNP-PEG-COOH in HP and 5 nm GNP-PEG-COOH in HP, 1% agarose gel electrophoresis was performed. The bands were cut, melted and treated using Agarase enzyme (EO0461 from Thermo Fisher Scientific). 1U of Agarose was added to 100 ul of melted agarose and incubated at 42º C for 30 min. The protein content was then denatured by boiling the samples for 5 minutes in loading buffer (62.5 mM Tris-HCl (pH 6.8), 2% (w/v) SDS, 10% glycerol, 0.01% (w/v) bromophenol blue, 40 mM DTT). So prepared samples, containing denatured proteins coated with SDS surfactant (which gives them negative net charge) were separated by size in the moiety of porous 10% polyacrylamide gel (1D SDS-PAGE), in electric field using a Mini-PROTEAN Tetra electrophoresis system from Bio-Rad.

SDS-PAGE (Sodium Dodecyl Sulfate Polyacrylamide Electrophoresis). For two running gels: 10 % SDS – PAGE gel was precast fresh before each experiment as 5.4 mL of MiliQ water, 2.5 mL of 1.5 M Tris – HCl buffer pH 8.9 and 0.1 mL of 10 % SDS are mixed well and 1.8 mL of 40 % acrylamide and 5 µL of TEMED were added and the solution was mixed again. As initiator, 50uL of 10 % ammonium persulfate were added. Gel solution is poured in the frame to polymerize. Stacking gels (4%) are made up with 0.5 mL acrylamide, 1.26 mL 0.5 M Tris-HCL buffer pH 6.8, 50 µL 10% SDS, 3.18 mL MiliQ water, 25 µL APS 10% and 5 µL TEMED and added on top of running gels.

The electrophoresis was run under constant voltage of 130 V for about 45 minutes. The gels were stained with 2D-SILVER STAIN-II reagents (Cosmobio Co.,Ltd) and scanned under white light using a G:Box Chemi XT4 (Syngene).

2.3.3 Mass spectrometry

For the LC-MS/MS analysis, the proteins of the corona complexes were first separated of the protein-NP complexes, by 10% Tris-Glycine SDS-PAGE gel. After running the electrophoresis under constant voltage of 140V for 10 minutes, the gel was stained with Commassie blue and the proteins bands taken from each lane prior to trypsin digestion and mass spectrometry. The gel section containing the proteins was removed using a sterile scalpel and transferred to a clean 0.5 mL sample tube which had been pre-rinsed with acetonitrile. The gel sections were trypsin digested in gel. The samples were resupended in 0.1% w/w formic acid prior to analysis by electrospray liquid chromatography (LC-MS/MS). All samples were run on a Thermo

Scientific LTQ ORBITRAP XL mass spectrometer connected to an Exigent NANO LC.1DPLUS chromatography system incorporating an auto-sampler**.** The raw mass spectral data have been searched against human protein database and analysed using MaxQuant® 1.4.1.2 software. A semi-quantitative assessment of the proteins amount was performed by the method of spectral counting (SpC), which represents the total number of the MS/MS spectra for all peptides attributed to a matched protein. The SpC of each protein identity was normalized to the protein mass and expressed as the relative protein quantity by applying the following equation (Eq.1):

$$NpSpC_k = \left(\frac{(SpC/M_w)k}{\sum_{i=1}^{n}(SpC/M_w)i}\right)x100 \qquad \text{[Eq.1]}$$

Where $NpSpC_k$ is the percentage normalized spectral count for protein k, SpC is the spectral count identified, and M_w is the molecular weight in kDa for protein k. The obtained results have been compared with the method of the label-free quantification (LFQ) performed by MaxQuant.[5] This method, able to accurately and robustly quantify small fold changes on a proteome scale, has the prerequisite that a majority population of proteins exists that is not changing between the samples therefore it has been applied to the samples incubated with the same serum at different percentages.

3 Supplementary Figures

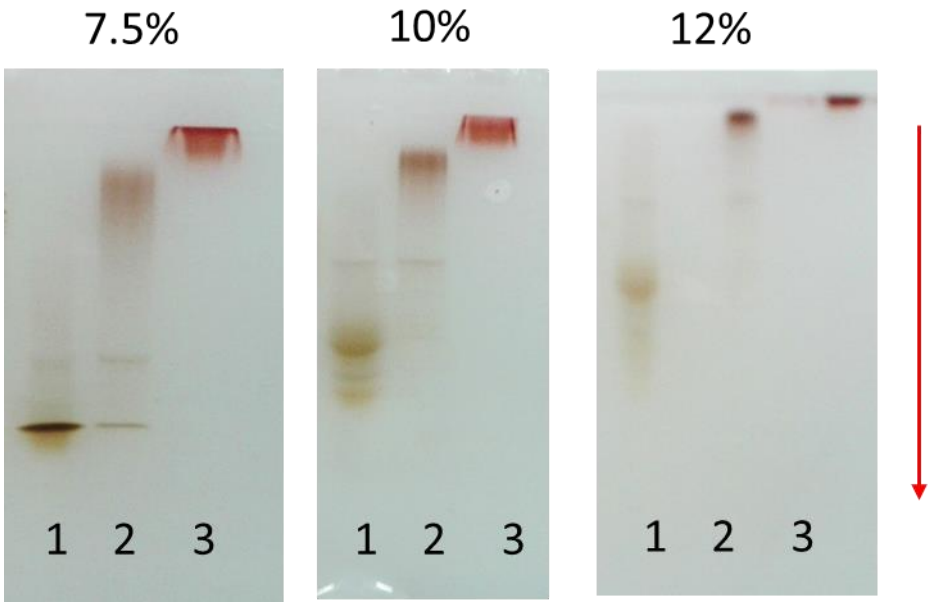

Figure S1. Size distribution investigation of GNP-PEG-COOH by polyacrylamide gel elecrophoresis: (1) 2 nm GNP-PEG-COOH, (2) 3 nm GNP-PEG-COOH, (3) 5 nm GNP-PEG-COOH.

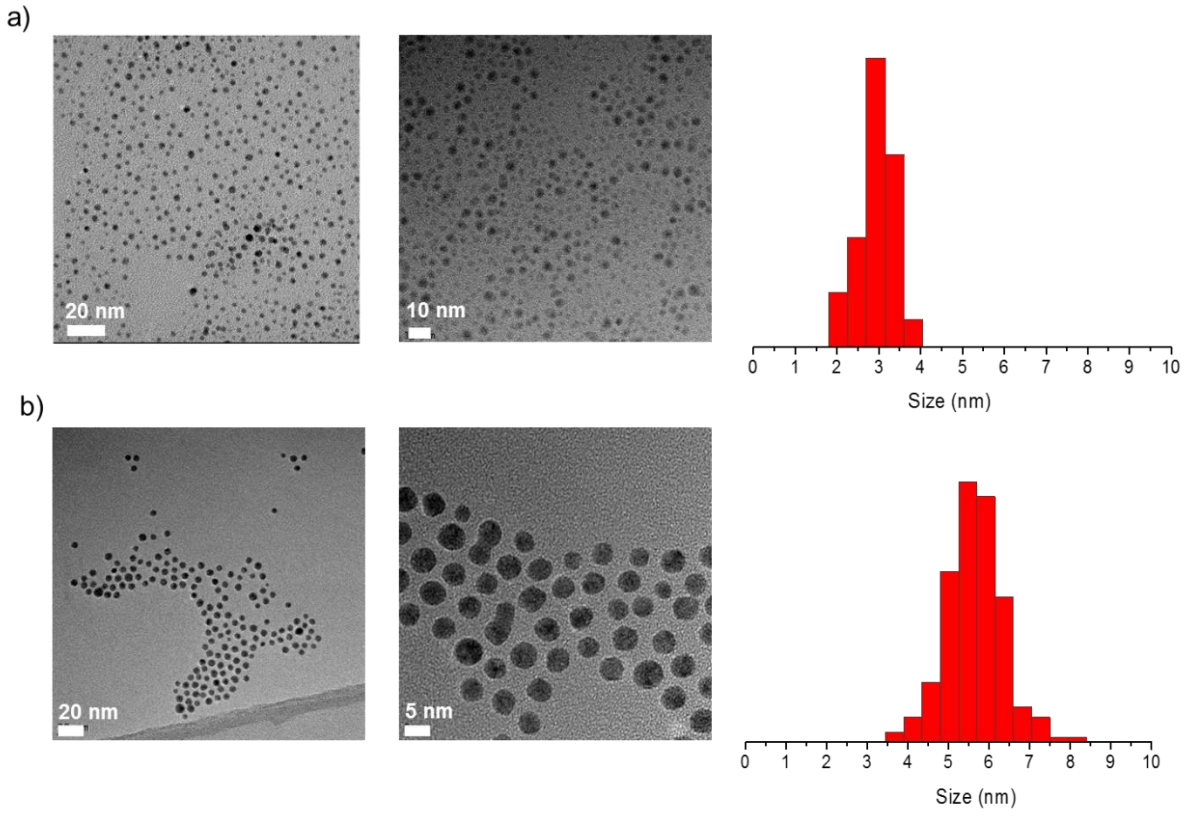

Figure S2. TEM micrographs and size distribution of 3 and 5 nm GNP-PEG-COOH.

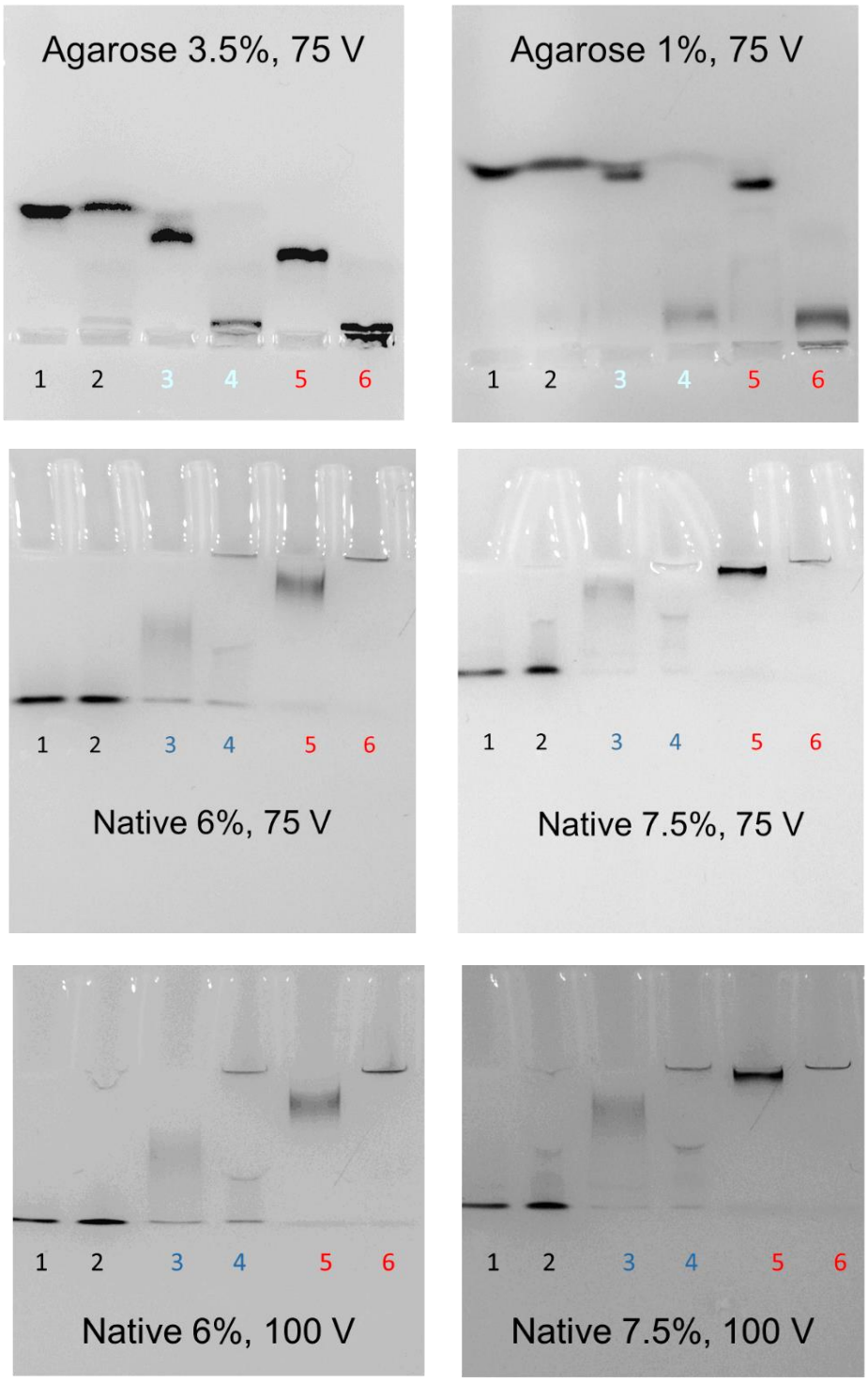

Figure S3. Different pore sizes of agarose and native polyacrylamide gel-assays in 1% native buffer. The numbered lanes refer 5 nm GNP-PEG-COOH in PBS (1) and in HP (2), 3 nm GNP-PEG-COOH in PBS (3) and in HP (4), 2 nm GNP-PEG-COOH in PBS (5) and in HP (6).

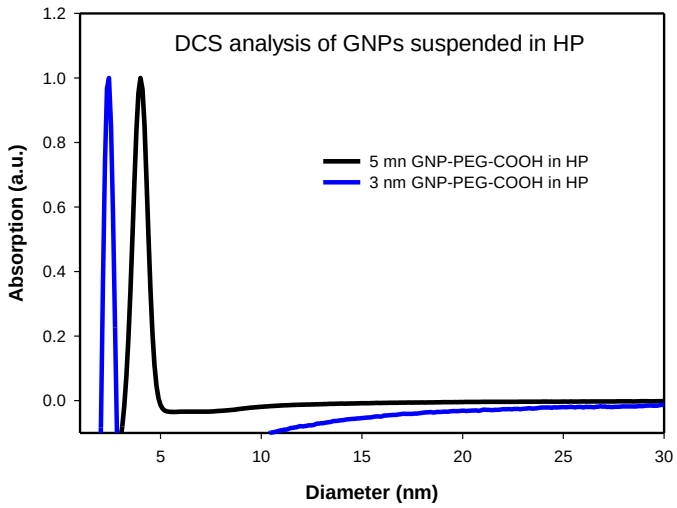

Figure S4. Stability test in human plasma by DCS. 5 nm and 3 nm GNP-PEG-COOH were suspended in HP and analysed by DCS. The sucrose gradient for this experiment was a PBS solution.

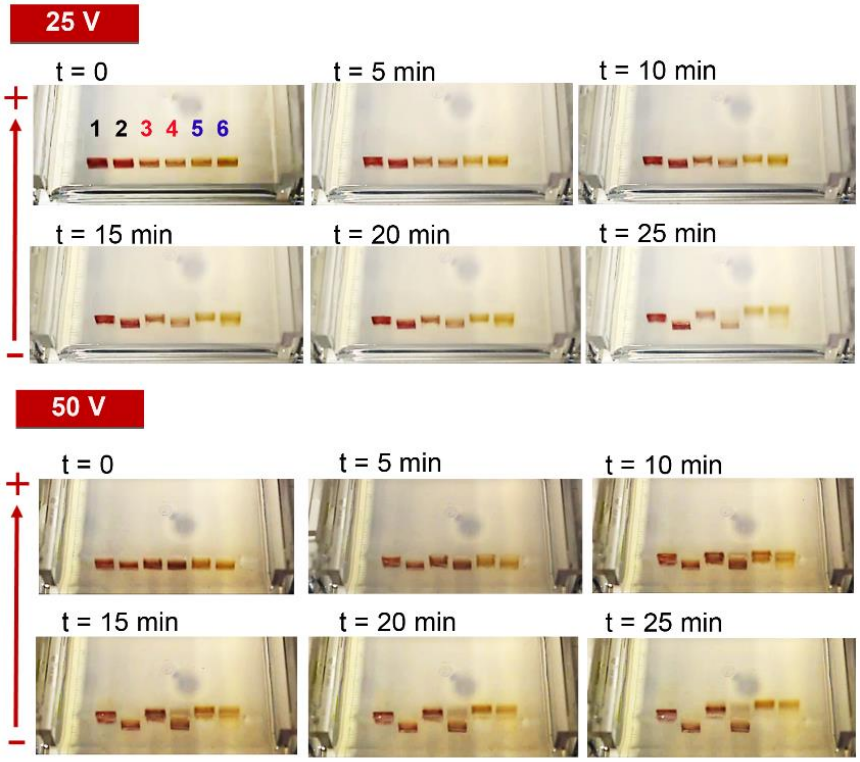

Figure S5. Endpoint images from the high resolution video of a 3.5 % agarose gel-assay experiment showing samples: 1) 5 nm GNP-PEG-COOH in PBS, 2) 5 nm GNP-PEG-COOH in HP, 3) 3 nm GNP-PEG-COOH in PBS, 4) 3 nm GNP-PEG-COOH in HP, 5) 2 nm GNP-PEG-COOH in PBS, 6) 2 nm GNP-PEG-COOH in HP. Running conditions: 25 V (above) and 50 V (below). The endpoint images demonstrate that the electrophoretic mobility of the NPs changes over time. In particular, 5 nm (lane 2) and 3 nm (lane 4) GNP-PEG-COOH in HP are significantly delayed in comparison to the NP control in PBS (lane 1 and 3 respectively). In

the first 15 minute of running it is possible to observe a small difference in the electrophoretic mobility also for the 2 nm GNP-PEG-COOH in PBS and HP (lane 5 and 6).

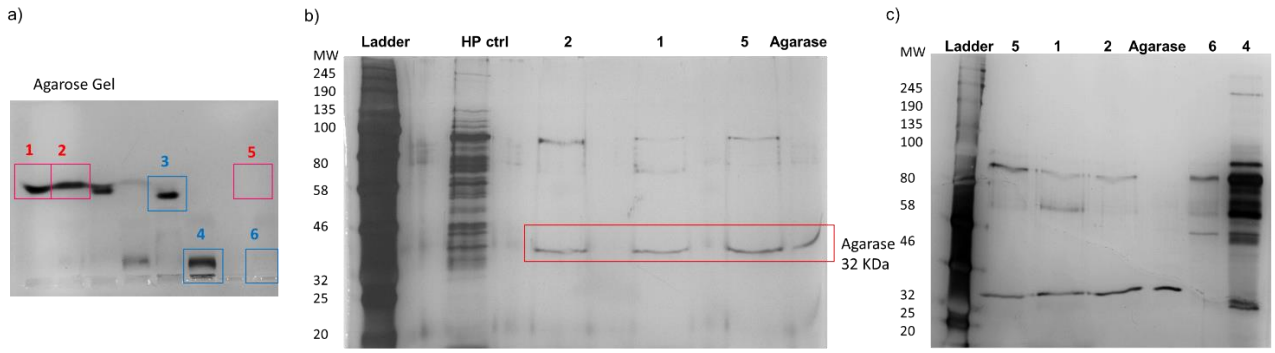

Figure S6. SDS-PAGE analysis of the different fraction recovered from the agarose gel electrophoresis. a) 1 % agarose gel-assay in a native buffer of 2 nm, 3 nm, and 5 nm GNP-PEG-COOH in PBS and in HP. Bands corresponding to 2 nm GNP-PEG-COOH in PBS (1) and in HP (2), 5 nm GNP-PEG-COOH in PBS (3) and in HP (4), and HP (5 and 6). b) and c) SDS-PAGE analysis of the nanoparticles and proteins recovered from the agarose gel.

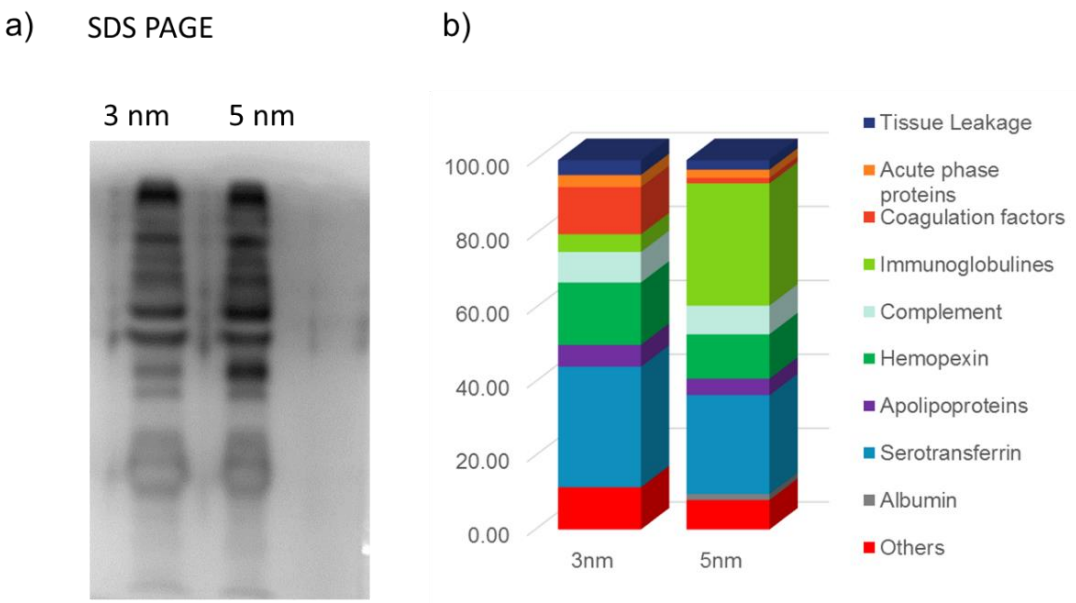

Figure S7. SDS-PAGE (a) and Mass spectrometry analysis (b) of protein corona of 3 nm and 5 nm GNP-COOH isolated by agarose gel electrophoresis.

Protein Name	NSpC (3nm)	Protein name	NSpC (5 nm)
Serotransferrin	10.13	Serotransferrin	6.01
Hemopexin	5.24	Hemopexin	2.70
Ig alpha-1 chain C region	1.29	Ig gamma-2 chain C region	1.49
Histidine-rich glycoprotein	1.00	Ig alpha-1 chain C region	1.05
Insulin-like growth factor-binding protein complex acid labile subunit	0.87	Retinol-binding protein 4	0.96
Retinol-binding protein 4	0.73	Ig kappa chain V-II region RPMI 6410	0.90
Serum amyloid P-component	0.69	Ig kappa chain V-I region AG	0.85
Complement factor B	0.67	Ig kappa chain V-II region TEW	0.75
Lumican	0.63	Beta-2-glycoprotein 1	0.74
Tetranectin	0.63	Ig heavy chain V-III region BUT	0.61
Kininogen-1	0.62	Ig lambda-3 chain C regions	0.61
Apolipoprotein A-IV	0.61	Ig lambda chain V-III region LOI	0.57
Complement factor I	0.60	Complement C1q subcomponent subunit B	0.56
Apolipoprotein C-III	0.58	Complement factor H	0.56
Coagulation factor XIII A chain	0.56	Complement factor B	0.55
WAP four-disulfide core domain protein 3	0.56	Serum amyloid P-component	0.50
N-acetylmuramoyl-L-alanine amidase	0.54	CD5 antigen-like	0.45
Apolipoprotein E	0.53	Ig lambda chain V-IV region Hil	0.44
Antithrombin-III	0.49	Insulin-like growth factor-binding protein complex acid labile subunit	0.44
Complement C3	0.48	Serum albumin	0.36
Kallistatin	0.46	Coagulation factor XIII B chain	0.33
Fibronectin	0.44	Apolipoprotein E	0.24
Carboxypeptidase B2	0.42	Pigment epithelium-derived factor	0.19
Complement factor H	0.40	Vitamin K-dependent protein S	0.17
Complement C5	0.38	Gelsolin	0.13
Alpha-1-antitrypsin	0.32	Ig lambda chain V-III region SH	0.13

Table S1. Mass spectrometry analysis of 3 nm and 5 nm GNP-COOH incubated with human plasma and isolated by agarose gel electrophoresis.

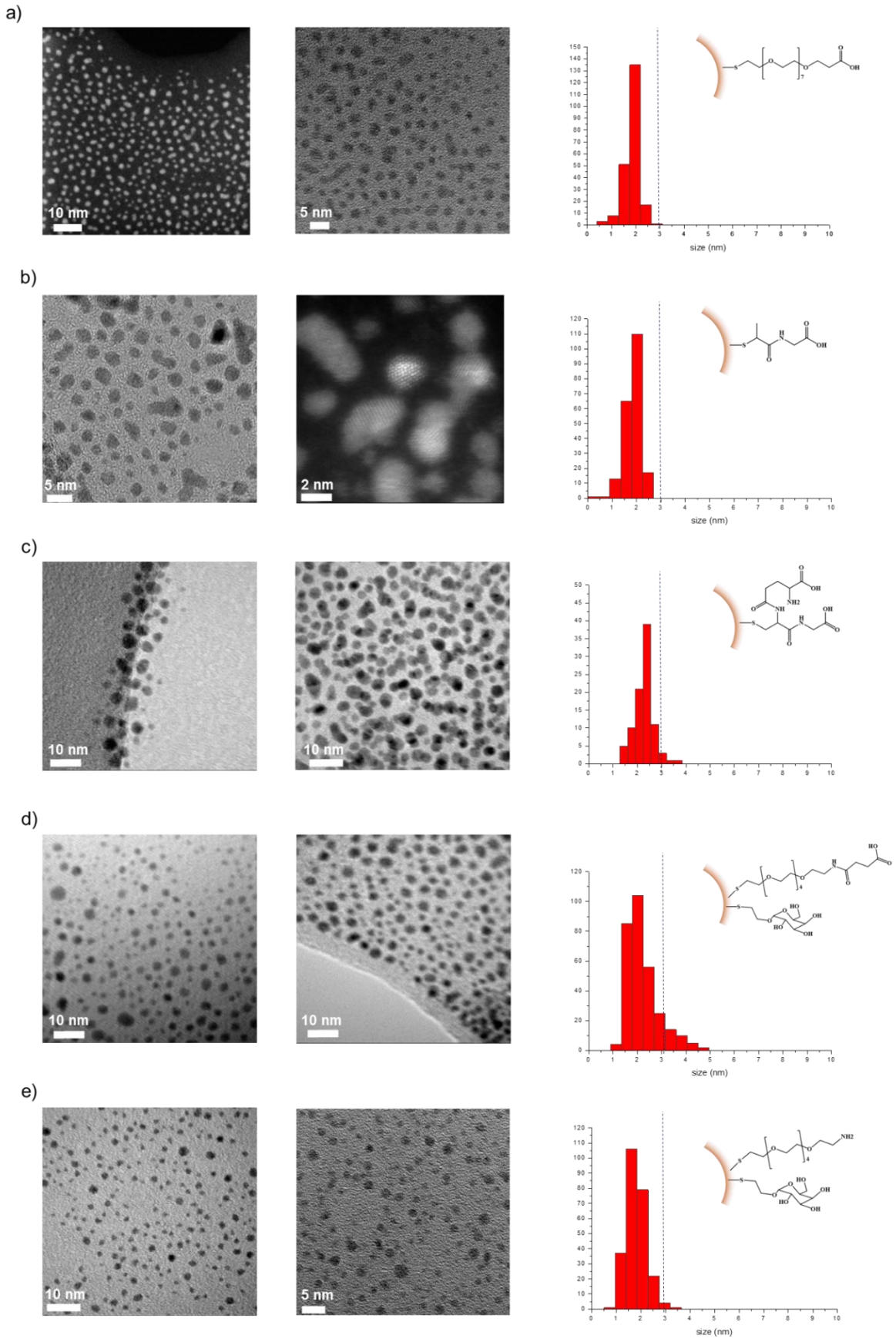

Figure S8. TEM micrographs and size distribution of 2 nm GNPs: a) GNP-PEG-COOH, b) GNP-tiopronin; the micrograph on the right shows individual gold atoms, c) GNP-glutathione

d) GNP-αGalPEGSuc, e) GNP- αGalPEGAmino. The dotted line shows that the nanoparticles distributions are centered around 2 nm and below 3 nm.

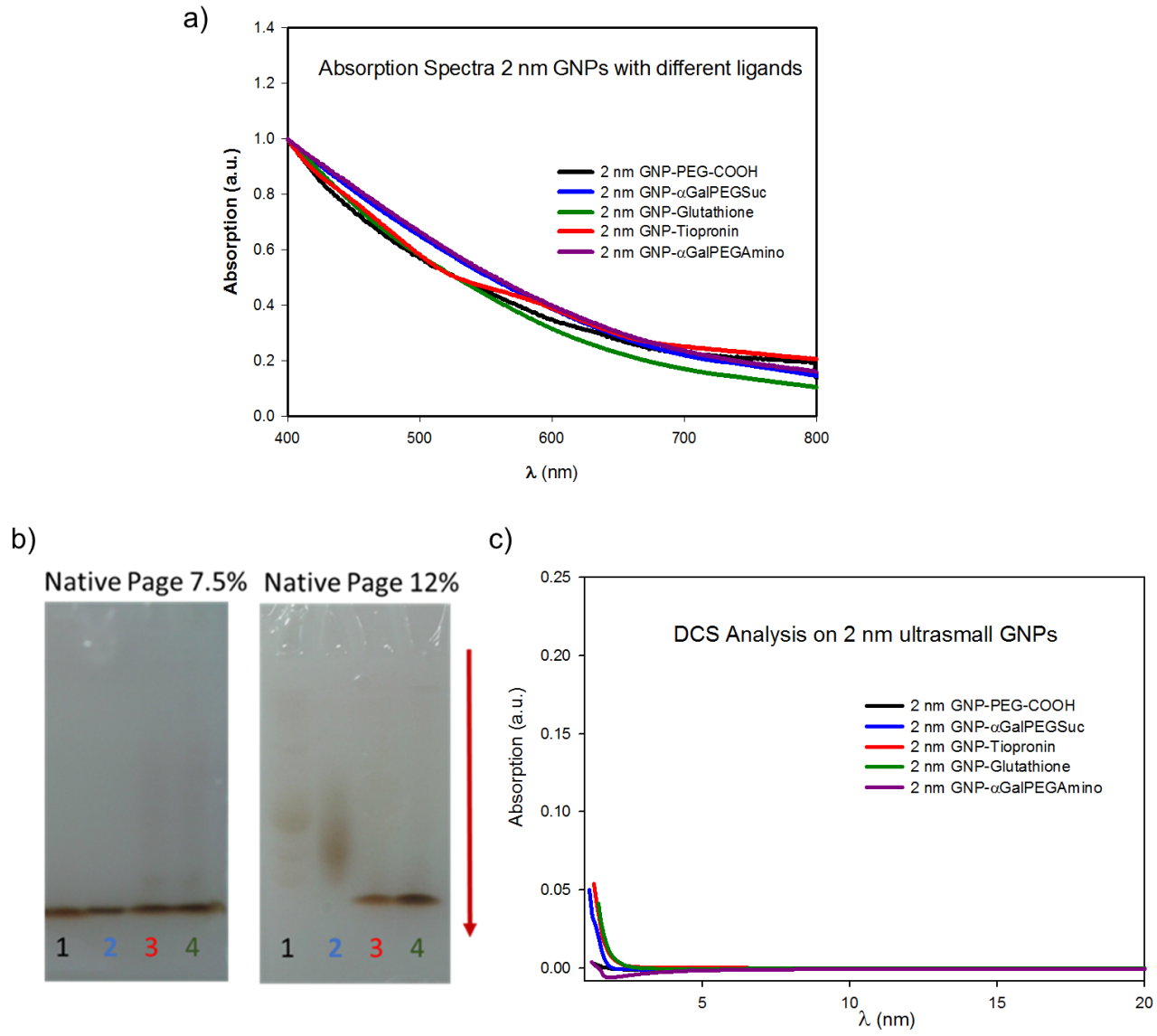

Figure S9. Characterization of 2 nm GNPs: a) DCS, b) Polyacrylamide gel electrophoresis: (1) GNP-PEG-COOH, (2) GNP-αGalPEGSuc, (3) GNP-tiopronin, (4) GNP-glutathione, c) UV-Vis spectroscopy.

1H-NMR of 5 nm GNP-PEG-COOH

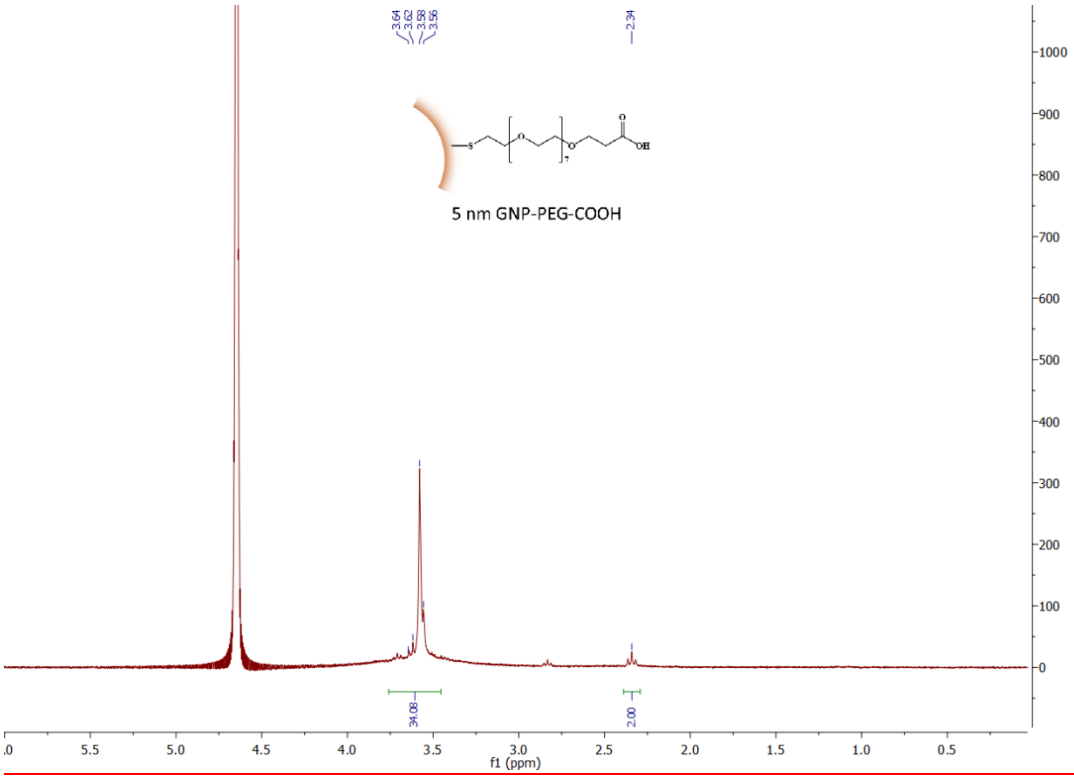

1H-NMR of 3 nm GNP-PEG-COOH

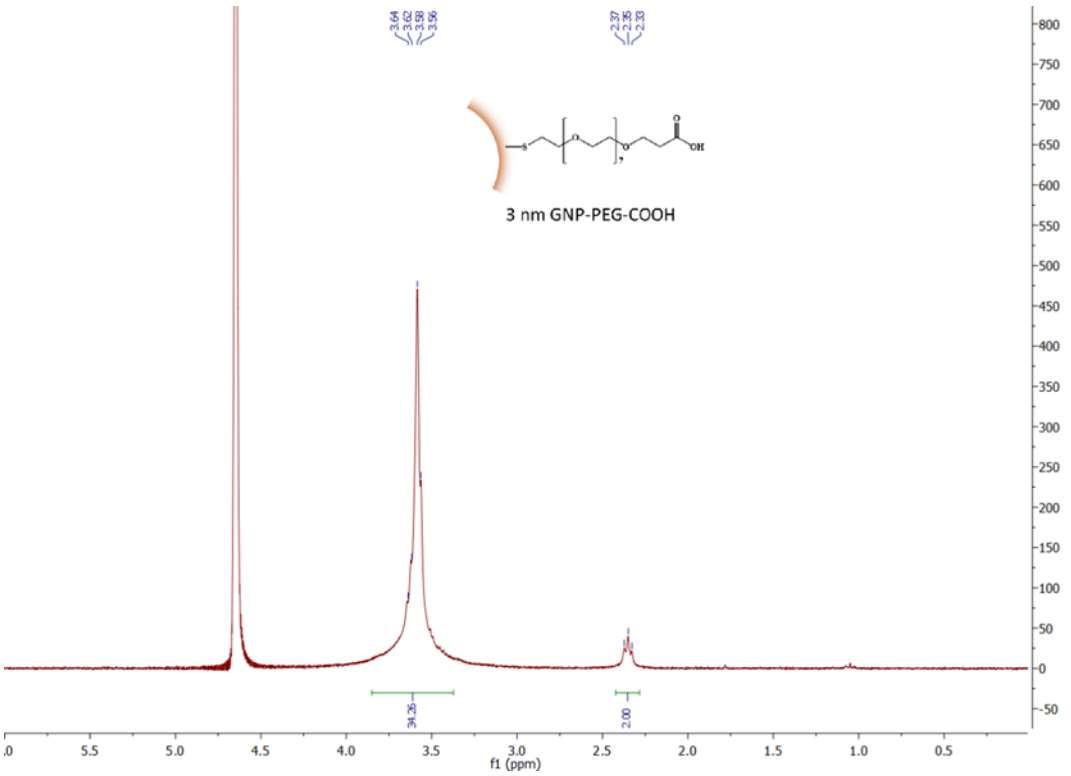

1H-NMR of 2 nm GNP-PEG-COOH

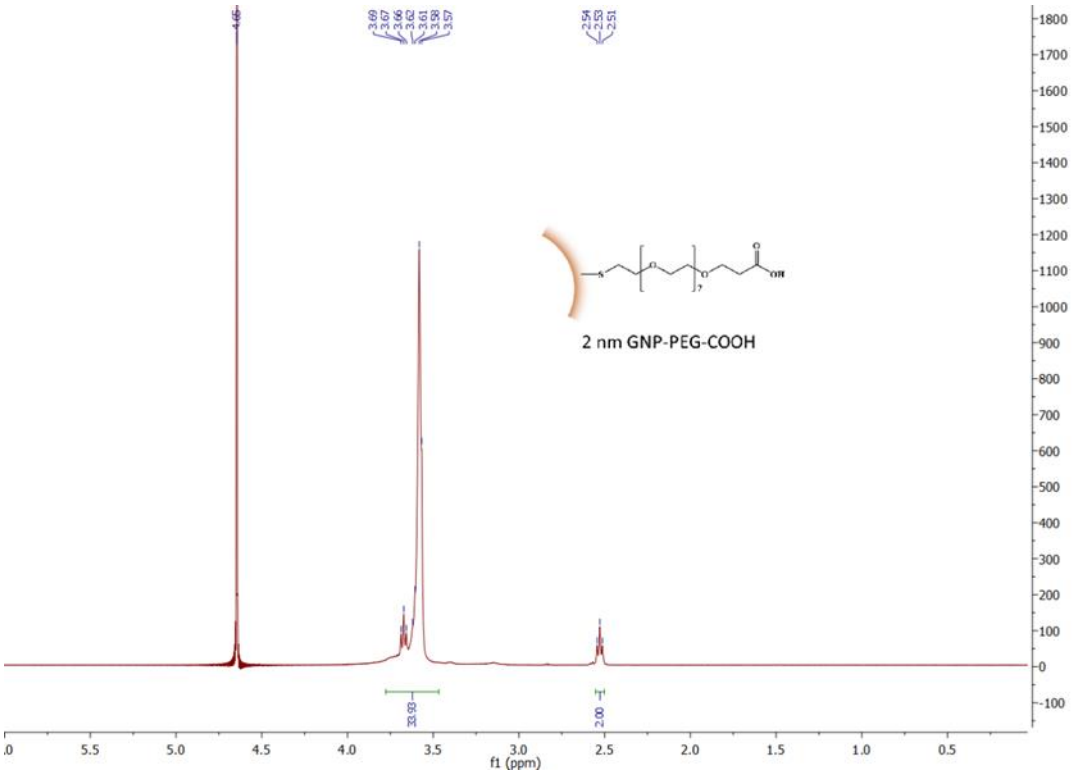

1H-NMR of 2 nm GNP-αGalPEGSuc

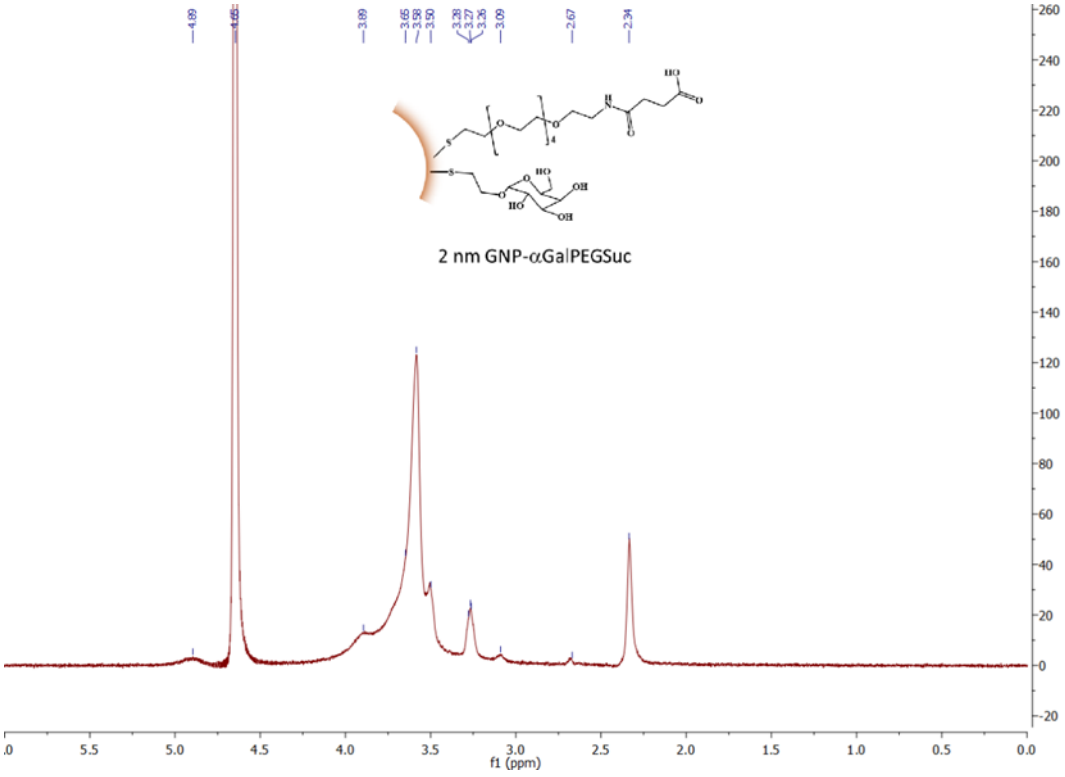

1H-NMR of 2 nm GNP-aGalPEGAmino

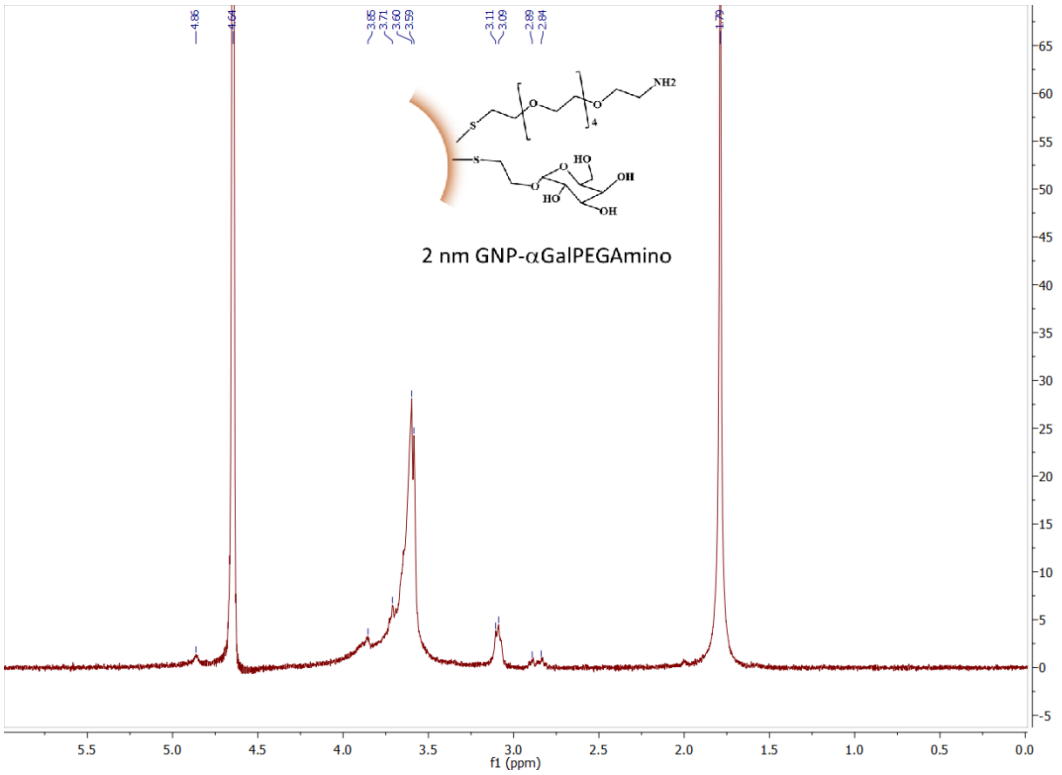

1H-NMR of 2 nm GNP-Tiopronin

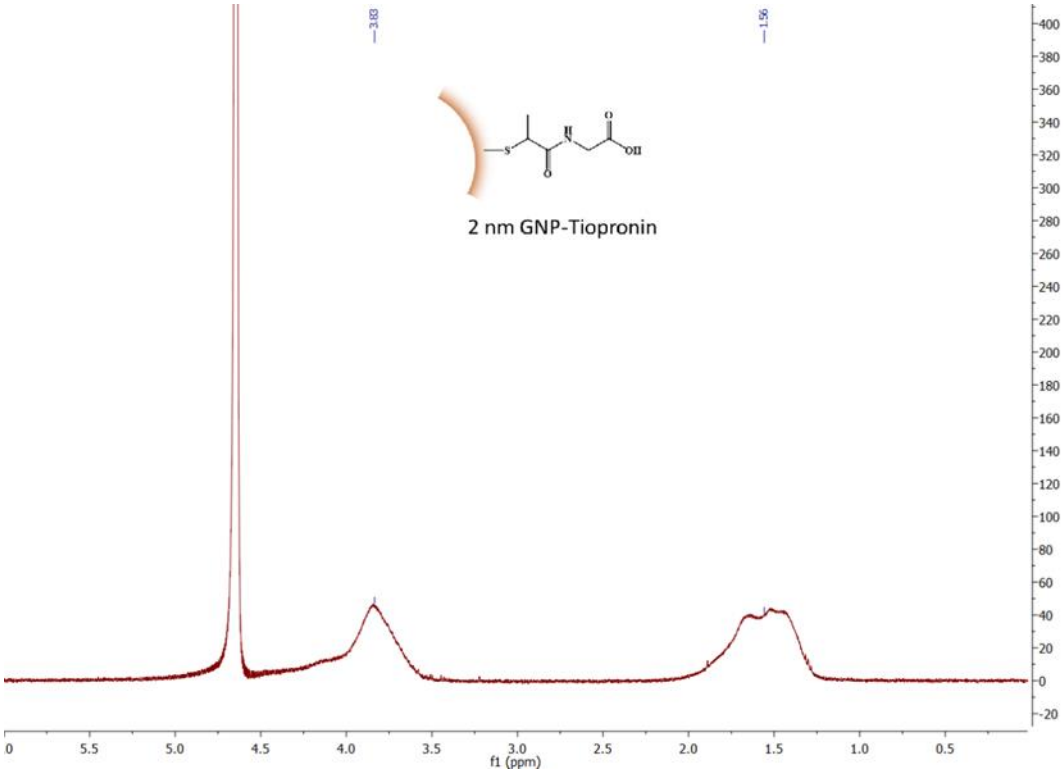

1H-NMR of 2 nm GNP-Glutathione

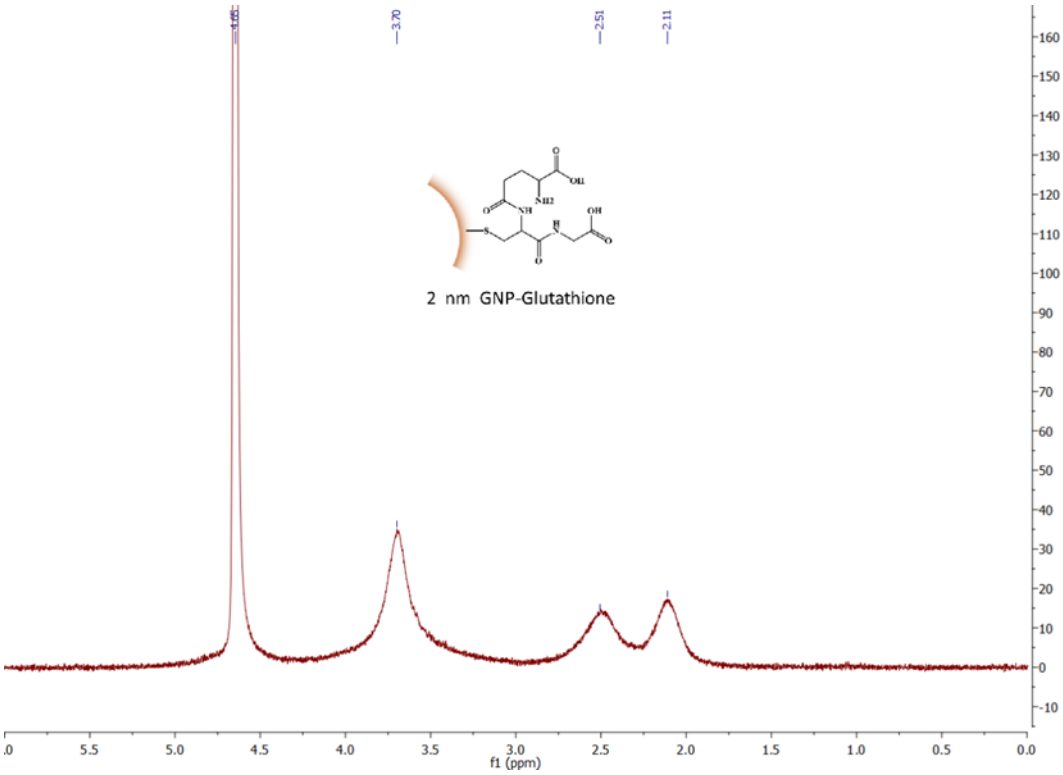

Figure S10. H-NMR spectra of different GNPs. ^{1}H-NMR spectra were recorded at 298 K in D_2O as solvent.[1,6,7]

Sample	TEM (nm)	Number particles	DCS (nm)	Z pot (mV)
5 nm GNP-PEG-COOH	5.2 ± 0.6	100	4.5 (RW)	-18 mV
3 nm GNP-PEG-COOH	3.0 ± 0.5	100	2.5 (RW)	-16 mV
2 nm GNP-PEG-COOH	1.9 ± 0.3	200	1 (RW)	-16 mV
2 nm GNP-Tiopronin	1.8 ± 0.3	200	1 (RW)	-27 mV
2nm GNP-Glutathione	2.3 ± 0.4	100	1 (RW)	-28 mV
2 nm GNP- αGalPEGSuc	2.0 ± 0.7	300	1 (RW)	-15 mV
2 nm GNP-αGalPEGAmino	1.8 ± 0.4	250	1 (RW)	+ 42 mV

Table S2. Summary of the GNPs characterization.

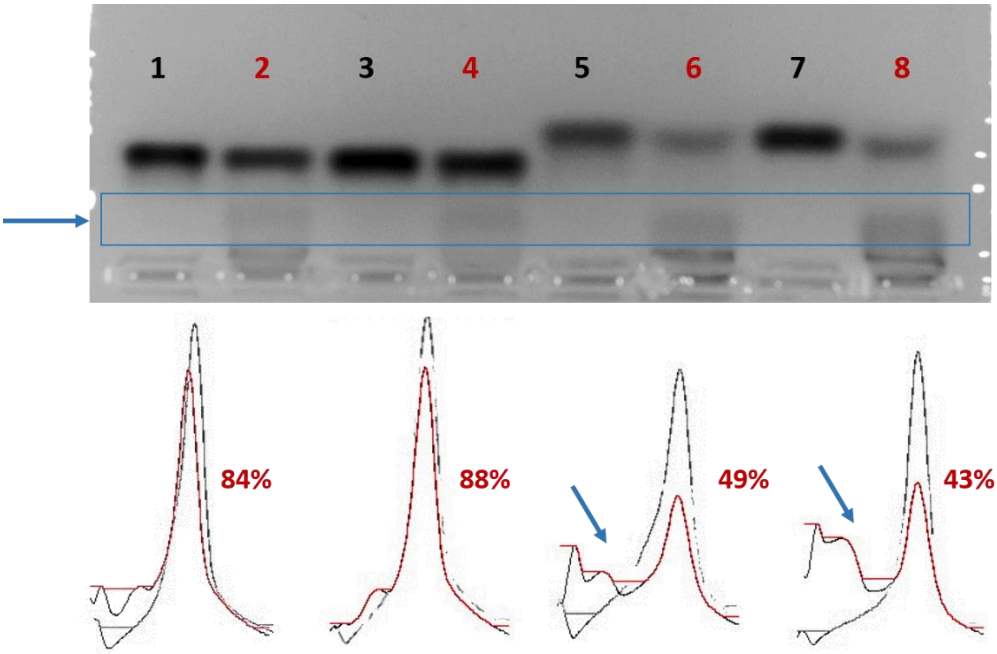

Figure S11. Densitometry of the agarose gel reported in Figure 4 (main text) showing 2 nm GNP-PEG-COOH in PBS (1) and in HP (2), 2 nm GNP- αGalPEGSuc in PBS (3) and in HP (4), 2 nm GNP-tiopronin in PBS (5) and in HP (6), 2 nm GNP-glutathione in PBS (7) and in HP (8). The densitometry analysis highlights a clear bimodal distribution for lane 6 and 8, due to partial interaction of the GNP-tiopronin and GNP-glutathione with the plasma proteins.

4 References

1. A.C. Templeton, S. Chen, S.M. Gross, R.W. Murray, *Langmuir* **1999,** *15* (1), 66-76.
2. J.W. Slot, H.J. Geuze, *Eur. J Cell Biol* **1985,** *38* (1), 87-93.
3. (a) J. Conde, P.V. Baptista, Y. Hernández, V. Sanz, J.M. de la Fuente, *Nanomedicine* **2012,** *7* (11), 1657-1666; (b) C. Parolo, A. de la Escosura-Muñiz, E. Polo, V. Grazú, J.M. de la Fuente, A. Merkoçi, *ACS Appl. Mater. Interfaces* **2013,** *5* (21), 10753-10759.
4. W. Haiss, N.T.K. Thanh, J. Aveyard, D.G. Fernig, *Anal. Chem.* **2007,** *79* (11), 4215-4221.
5. J. Cox, M. Mann, *Nat. Biotechnol.* **2008,** *26* (12), 1367-1372.
6. P. Pengo, S. Polizzi, M. Battagliarin, L. Pasquato, P Scrimin, *J. Mater. Chem.,* **2003**,13, 2471-2478
7. T. G. Schaaff , G. Knight, M.N. Shafigullin, R.F. Borkman, R. L. Whetten *J. Phys. Chem. B*, **1998**, 102 (52), pp 10643–10646